RSC Advances

ROYAL SOCIETY OF CHEMISTRY

www.rsc.org/advances

Role of polymeric surfactant in the synthesis of cobalt molybdate nanospheres for hybrid capacitor applications

Maryam Jozegholami Barmi and Manickam Minakshi Sundaram*

School of Engineering and Information Technology, Murdoch University, WA 6150, **Australia**

Abstract

The role of Pluronic F127, a tri-block copolymer i.e. poly(ethylene oxide) – poly(propylene oxide) – poly(ethylene oxide) PEO – PPO – PEO, onto cobalt molybdate ($CoMoO_4$) and its influence on the physico-chemical properties have been investigated. Surfactants are molecules able to alter the surface properties of the $CoMoO_4$ during the synthesis. Through a facile synthesis at 300 ^oC, F127 adsorbs at the interface and self-assemble into a micellar aggregate resulting in the formation of $CoMoO_4$ nanospheres. A cluster of nano-particles with an average size of 250 nm are obtained for F127 added $CoMoO_4$, while rod shaped particles (1 µm) are obtained in the absence of F127. The surfactant assisted $CoMoO_4$ is associated with enhanced pore accessibility and electronic conductivity, having a dual role in offering potential applications. The objective of this study is to test the as-synthesized $CoMoO_4$ for energy storage application by tuning the surface properties. The hybrid capacitor (F127 added $CoMoO_4$ *vs.* activated carbon) showed excellent electrochemical performance with specific capacitance of 79 F g^{-1} and energy density of 38 Wh · Kg^{-1} in 2 M NaOH electrolyte which was much higher than that for pure $CoMoO_4$ (23 F g^{-1}). Long term cycling stability of the modified $CoMoO_4$ was tested and found almost 80% of its initial capacity retained after 2000 cycles. The obtained results suggest the F127 added $CoMoO_4$ be a suitable candidate to fabricate a cost effective energy storage device.

***Keywords*:** Cobalt molybdate; surfactant; polymer; nanospheres; synthesis.

*E: *m.minakshi-sundaram@murdoch.edu.au* T: +61 (8) 9360 2017

1. Introduction

A water soluble, Pluronic (F127) poly(ethylene oxide) – poly(propylene oxide) – poly(ethylene oxide) PEO – PPO – PEO, tri-block copolymers are known to adsorb onto molybdenum species such as cobalt molybdate ($CoMoO_4$). Above the critical micellization concentration (CMC), the added F127 tri-block copolymer form micelles and self-assemble into a variety of aggregations. The role of polymeric surfactant onto $CoMoO_4$ during the synthesis and its effect in physico-chemical and electrochemical properties have been studied for the first time. Such studies on the interactions between the polymer and $CoMoO_4$ morphology provide fundamental insights on the surface properties and its use in energy storage applications.

Electrochemical supercapacitors possessing rapid charging, excellent cycling stability, and of miniature in size are attractive features for next generation power devices [1]. However, electrochemical capacitors suffer from low energy density compared to rechargeable battery systems [2]. Until now, much work has been devoted to improve the energy density of capacitors to meet the demand for next generation supercapacitor applications [3-4]. Commercial supercapacitors are comprised of two identical activated carbon (AC) electrodes. These supercapacitors are of the electrical double layer capacitors (EDLC) type. Being fully dependent on double layer, these supercapacitors suffer from poor energy density (5-6 $Wh \cdot Kg^{-1}$) [5]. To overcome this, efforts have been taken to investigate and study the electrochemical properties of supercapacitors based on dissimilar electrodes such as activated carbon (AC) negative electrode and metal oxide positive electrode [6-9].

There are a range of candidates that can be employed as electrodes for batteries and supercapacitors. Transition metal oxides (RuO_2, MnO_2) [10-12] and phosphate materials ($LiNiPO_4$, [13] $LiCoPO_4$, [14] $LiMnPO_4$ [15]) were widely studied and following to this, recently there has been a renowned interest in molybdates. Transition metal in oxides and

phosphates played an important role in tuning the redox potential that resulted in improved performance characteristics of the energy storage devices [10-15]. Various transition metal oxides have been proposed for application in supercapacitors. Among them, ruthenium oxide exhibits high capacitance, good electrochemical properties and excellent reversibility. However, its application is limited due to high cost and low porosity [10]. Subsequently, manganese dioxide (MnO_2) is considered to be another promising candidate for supercapacitors for its high energy density and low cost. But, MnO_2 has been plagued due to its poor cycling stability and poor electrical conductivity [12]. Thereon, research has been focused on overcoming the disadvantages of MnO_2 by introducing different additives to the active MnO_2 material [15]. On the other hand, phosphate materials are quite poor in terms of conductivity.

Alternatively, it is well known that molybdate materials have excellent catalytic activity, good electrochemical properties, and environmentally friendly [2]. Due to these specifications, a lot of efforts have been made to study the possibility of using metal molybdates in energy storage devices [6-9], [16-20]. Among various molybdate materials, $MnMoO_4/CoMoO_4$ heterostructured nanowires showed specific capacitance of 187 F g^{-1} at current density of 1 A g^{-1} with an excellent reversibility after 1000 cycles. These nanowires were reported to have larger surface area and defects that promoted good electron transport and efficient electrochemical reactions [1]. A $CoMoO_4$ nanoplate exhibiting a capacitance of 170 F g^{-1} over 1000 cycles has also been reported [16]. In another work, $CoMoO_4$ nanoplates synthesised via hydrothermal route has shown specific capacitance of 1.26 F cm^{-2}. The reported performance was correlated to the open network structure of $CoMoO_4$ coated on Ni foam [21]. Following this, Xu et al [17] reported an increase in electrical conductivity of $CoMoO_4$ composite material through an in-situ addition of graphene that resulted in a specific capacitance of 322 F g^{-1}. Apart from the single cell characteristics, asymmetric

hybrid device constructed from AC and $CoMoO_4$ in 2 M LiOH has also been reported with a specific capacitance of 105 F g^{-1} [18]. However, the fabricated hybrid device has resulted in meagre energy density of 14 W h Kg^{-1}. More recently, $NiMoO_4$@$CoMoO_4$ nanospheres were synthesised through hydrothermal technique [22]. Zhang's group have shown the nanospheres exhibiting a specific capacitance of 77 F g^{-1} at a current density of 14 A g^{-1} when tested for symmetric capacitor device [22]. The enhanced electrochemical properties of the material compared to pure $CoMoO_4$ material was attributed to the fast diffusion of ions resulted from the effect of Ni and Co molybdates deposited onto a conductive substrate [22]. Overall, almost all the reported work on $CoMoO_4$ material has been focused on conventional synthetic methods such as microwave, combustion, hydrothermal, co-precipitation *etc*. and tested for single electrode characteristics employing cyclic voltammetric technique. In addition, the working potential window of most of the reported materials is limited which affects their application in energy storage. No work has been done so far on the influence of polymeric surfactants and its micellar formation that resulted in nanocomposites which is a prerequisite for capacitor applications. The employed one-step facile approach in our work is cost-effective and scalable for commercialization.

Herein, we successfully prepared an asymmetric hybrid device comprising AC|| α-$CoMoO_4$. To the best of our knowledge, this is the first time an asymmetric AC|| α-$CoMoO_4$ full cell has been built in an aqueous system and tested in galvanostatic conditions, in which a unique polymeric surfactant (Pluronic F127) is employed. The tri-block copolymer surfactant F127 belongs to a group of commonly used water–soluble surface active compounds. The objective of having surfactant during the chemical synthesis is to achieve (a) nanostructured morphology through the aid of structure directing agent such as F127, (b) enhance the adsorption properties of F127 onto $CoMoO_4$ which controls the shape of the micelles and their interaction with the molybdate species and (c) have a uniform distribution of conductive

carbon in the $CoMoO_4$ matrix to achieve a better conductivity. This enhances the effective electrolyte diffusion and charge transport resulting in improved specific capacitance and rate capability. Aqueous systems are a preferable electrolyte choice for a number of reasons. They are far less expensive than organic solvents and have fewer disposal and safety issues. The ionic conductivity of NaOH (aq.) is two orders of magnitude greater than that of organic electrolytes, allowing higher discharge rates and lower voltage drops due to electrolyte impedance. Hence, a solution of 2 M NaOH (aq.) was used as an electrolyte in the current asymmetric capacitor study.

2. Experimental

2.1 Materials

Cobalt molybdate (α-$CoMoO_4$) was synthesised using analytically pure Co $(NO_3)_2.6H_2O$ (6.648 g), $(NH_4)_6Mo_7O_{24}.4H_2O$ (4.033 g) and 1.7 g Pluronic F127 known as F127 supplied by Sigma Aldrich. Pluronic F127 poly (ethylene oxide) – poly – (propylene oxide) – poly (ethylene oxide) block copolymer has M_W =12600 with 70% PEO content. The formula for this copolymer is $EO_{106}PO_{70}EO_{106}$. For comparison purposes, $CoMoO_4$ in the absence of surfactant was also synthesised. Details of the synthesis procedure are given in our previous work [18]. Figure 1 shows the schematic diagram for synthesis of $CoMoO_4$ in the presence of F127 surfactant. Activated carbon (AC) is commercially bought from Calgon Carbon.

2.2 Characterization

Modified $CoMoO_4$ sample was characterised by physical characterisation methods and compared to those of pure sample. The physical and electrochemical characterisations of the activated carbon are given in detail in Figs. S1 – S3 (ESI[§]). XRD was used to identify the crystal structure of prepared materials using Siemens D 500 X-ray diffractometer 5635 with a Cu-Kα source at a scan speed of $1^o\,min^{-1}$. The voltage and current were 35 kV and 28 mA, respectively. In addition, Attenuated Total Reflectance Fourier Transform Infrared (ATR-

FTIR) studies were employed using a Bruker IFS 125/HR spectrometer at Australian Synchrotron to study the nature of bonding and chemical structure of the modified $CoMoO_4$. Far IR and Mid IR pellets were prepared mixing samples with Paraffin and KBr, respectively. A high magnification Zeiss Neon 40ESB Field Emission Scanning Electron Microscope (FE-SEM) instrument was also used to acquire topographical and elemental information of the samples prepared. The morphology and lattice imaging of the $CoMoO_4$ powder were characterised by transmission electron microscopy (TEM), using a JEOL 200F TEM operated at 200 kV. TEM specimens were prepared by grinding a small amount of powder under methanol and dispersing on a holey carbon film. Brunauer, Emmett and Tellet (BET) surface area measurements and porosity analysis were also carried out by Micromeritics Tristar II surface area and porosity analyser. For porosity measurements, all samples were degassed at 100^{o} C overnight before analysis. For the three-electrode tests, a platinum wire of 10 cm length and 1 mm diameter and mercury–mercuric oxide (Hg/HgO) served as the counter and reference electrodes, respectively. The capacitor device was constructed with cobalt molybdate as the positive electrode and activated carbon as the negative electrode.

2.3 Device Fabrication and Measurements

For electrochemical measurement, the positive and negative electrodes were prepared by mixing either $CoMoO_4$ or AC (75 wt. %), carbon black (15 wt. %) and PVDF (10 wt. %) with 0.4 mL of NMP to make slurry. The slurry was coated on a small graphite sheet (area of coating, 1 cm^2). The remainder of the graphite strip was thoroughly masked using an insulation film to obtain a coated surface area of 1 cm^2 exposed to the 2 M NaOH electrolyte. Cyclic voltammetry of the samples were carried out using an EG&G Princeton Applied Research Versa Stat III model. In the case of single electrode characteristics, for cyclic voltammetry (CV) tests, the working electrode was cycled between 0 and 0.65 V at scan rates of 1, 2, 5 and 10 mV s^{-1}. Galvanostatic charge-discharge cycles were performed in the

identical potential range as that of CV test but using an 8-channel BioLogic VSP-300 battery analyser from MTI Corp., USA at a current density of 0.1 A g^{-1}. For AC, the working electrode was cycled between 0 and -1.0 V at a scan rate of 2 mV s^{-1}. The mass balance was calculated using the equation (1)

$$m+ /m- = (C_- * \Delta E_-) / (C_+ * \Delta E_+) \qquad \text{Eq. (1)}$$

where C_- and C_+ the specific capacitance for the AC and $CoMoO_4$, respectively; ΔE_- and ΔE_+ the potential difference from the open circuit voltage (OCV) to the AC and $CoMoO_4$ charge - discharge potential stability limits, respectively.

The specific capacitance of the AC and $CoMoO_4$ after subtracting from contributions of carbon black (acetylene black) and binder were calculated to be 135 F g^{-1} and 170 F g^{-1} respectively. Based on the single electrode characteristics, from the above equation (1), the optimal mass ratio between AC and $CoMoO_4$ was determined to be 1.6 for the fabricated hybrid capacitor. Therefore, the mass of the AC and $CoMoO_4$ material was 16.0 and 10.0 mg, respectively. An aqueous solution of 2 M NaOH was employed as an electrolyte for all electrochemical measurements. A hybrid capacitor has been fabricated and the charge–discharge studies were carried out at various current densities ranging between 0.1 and 1.0 A g^{-1}. The cut-off charge and discharge voltages were 1.6 and 0.2 V, respectively. Specific capacitance and energy density of the device were calculated at the end of each charge-discharge test. Electrochemical impedance spectroscopy (EIS) was carried out with amplitude of 5 mV over a frequency range of 10 mHz to 700 KHz at open circuit potential.

3. Results and Discussion

3.1. Physico-chemical characterization of $CoMoO_4$

The synthesis of cobalt molybdate ($CoMoO_4$) was performed using a cost-effective one-step, polymeric surfactant assisted combustion method. The synthesized $CoMoO_4$ were analysed

for crystal structure and phase determination using X-ray diffraction (XRD) technique. The X-ray diffraction (XRD) patterns of both the pure and modified (F127 added) $CoMoO_4$ samples are in good agreement with the reported values [18] and Powder Diffraction File (PDF) card number 21-0868 indicating the formation of single phase crystalline structure $CoMoO_4$. A typical diffraction pattern for modified $CoMoO_4$ is shown in Fig. 2. The pattern represents one major peak at 26.5^o (220) along with several minor peaks labelled in the figure. The absence of any secondary phases confirms the modified $CoMoO_4$ is of high purity. The crystallite size of 9.5 nm was calculated by the Debye-Scherer formula using the major diffraction peak (220) having full-width at half-maximum (FWHM) as 0.9^o.

Figure 3 shows the far and mid IR spectra of the modified $CoMoO_4$. To the best of our knowledge, the far IR region has not been reported earlier for $CoMoO_4$ material in the literature. The absorption band observed (Fig. 3A) at 433 cm^{-1} and several other shoulder like regions corresponds to the Co-Mo-O bands. However, in this study, no attempts are made to characterise these bands observed in Fig. 3A by assigning frequencies of *M* – O, *M*- *O*- *M*, or *M* – *M* (where *M* indicates Co and Mo and O indicate oxygen) as no database is available. In the mid IR region (Fig. 3B), peaks observed at 710, 760, 855, 950, 1400, 1600, 2220, 2354 and 3350 cm^{-1} are in good agreement with the reported values of $CoMoO_4$ [5, 6, 19, 20]. The peaks in the region 700-950 cm^{-1} corresponds to Mo-O bonds while the peak at 1400 cm^{-1} is related to MoO_4. To further explore the adsorption characteristics of the modified $CoMoO_4$, the obtained spectra for the mid infra-red region was compared with the pure $CoMoO_4$. The differences in the mid - infra red region is shown in Fig. S4 (ESI[§]). The IR spectrum of pure $CoMoO_4$ showed strong peaks at 1300, 1500 cm^{-1} and a band at 3400 cm^{-1} implying the characteristic absorption peaks for $CoMoO_4$. The band at 3400 cm^{-1} could be assigned to O-H bonds. While for modified sample, an intense peak at 1620 cm^{-1} and a band at 3250 cm^{-1} region with a high intensity have been observed. The observed peak shifts in the two spectra

could be attributed to the adsorption of non-ionic surfactant from the precursor solution onto molybdate species involving hydrogen bonding [23]. The peak at 1620 cm^{-1} can be assigned to the Mo^{6+} −OH bending vibrations. A band at 3250 cm^{-1} can be attributed to the hydrogen bonded water molecules adsorbed on the surface of $CoMoO_4$ [24]. Overall, the IR results suggest that the adsorption occurred mainly via hydrogen bonding between the oxygen atoms of the hydrophilic chain in F127. The XRD pattern and IR results suggest that the obtained product is $CoMoO_4$ and the bonding variation is confirmed for the surfactant modified sample. However, information about the formation of nanostructure, its chemical composition, adsorption properties *etc*. cannot be gained.

3.2 Morphological studies of $CoMoO_4$

(a) FESEM Studies

Microscopic analyses provide vital information on the size, homogeneity and intermolecular aggregation of modified $CoMoO_4$. The Field Emission SEM (FE-SEM) images of the pure and modified samples are compared in Fig. 4. The elemental analysis corresponding to $CoMoO_4$ samples depicted from Fig. S5 (ESI[§]) confirms the presence of mainly Co and Mo. As can be seen from the FE-SEM images, there is a significant change in morphology when polymeric surfactant was added onto $CoMoO_4$ during the synthesis. The pure $CoMoO_4$ show rod-like morphology (Fig. 4A-B) fused together while the modified $CoMoO_4$ (Fig. 4C-D) show clusters of nano-particles with an average size of 250 nm (with an individual crystallite size of ~10 nm) forming nanospheres. The observed trend is a typical behaviour of F127 having a tendency to self-assemble into a variety of micellar aggregations forming nanostructures due to the increased size of PEO blocks [25]. A similar kind of spherical mesopores was observed for silica composites synthesised using Pluronic F127 [26]. The modified sample shows the nanostructured particles that are highly porous in nature. The presence of micelles and $CoMoO_4$–surfactant interactions favoured by the given synthetic

temperature, allows the formation of nano-spherical shaped particle (see Fig. 1). The irregular shape seen in Fig. 4C-D indicates the micelles are becoming unstable at 300 ^{o}C and unable to template a regular pattern of spherical in nature. The elemental composition of the modified sample (Fig. S5 (ESI[§]) showed a carbon peak confirming the distribution of residual carbon decomposed from the F127 surfactant obtaining $CoMoO_4$/C nanocomposites. The formation of mesopores and carbon that facilitates fast ionic diffusion with reduced internal assistance [27] acts as a dual role for improved specific capacitance of the modified $CoMoO_4$ material. As a result, it can be concluded that morphology and pore accessibility of the sample can be altered by the addition of F127 surfactant. The synthetic temperature and concentration of surfactant which are the main parameters to modify the poly-ethylene-oxide chains in the product and its degradation will be discussed in detail in our subsequent publication.

(b) TEM imaging

To further confirm the morphology and its lattice imaging, transmission electron microscopy associated with energy dispersive X-ray spectroscopy (EDS) have been performed and the corresponding images are shown in Fig. 5 and Fig. S6 (ESI[§]). The observed differences in the imaging ascertain the change in morphology of $CoMoO_4$ samples in the presence and absence of F127 surfactant which is well agreeing with the SEM images observed in Fig. 4. Rod like particles of 0.5 µm are observed for pure $CoMoO_4$ as can be seen from Fig.5 A-B under different magnifications. Pure $CoMoO_4$ showed a blend of porous and non-porous crystals with a particle size ranging from 100 – 600 nm. In the case of modified $CoMoO_4$ (Fig. 5C), it showed a cluster of particles of around 200 nm possessing nano spherical particles which are uniformly distributed and porous in nature. Interestingly, Fig. 5D of the TEM imaging shows a region corresponding to a hexagonal pattern of the obtained $CoMoO_4$ product. The corresponding lattice fringes of the imaging in Fig. 5D (inset) exhibits the spacing distance of 0.3 nm which can be indexed to the (220) plane of $CoMoO_4$ and this in a good agreement

with XRD results. The TEM/EDS approach has been employed to quantitatively analyse the chemical composition of the $CoMoO_4$ sample. The TEM imaging and its composition profile are shown in Fig. S6 (ESI[§]). The spectra analysed at different locations in the samples invariably showed the presence of Co, Mo and O. However, for the modified $CoMoO_4$ sample, the composition of Mo has been decreased suggesting the F127 surfactant adsorbed on the molybdate moiety. The morphological studies confirm that the pure and modified $CoMoO_4$ are quite distinct in terms of surface chemistry. It is expected that the modified material can improve the adsorption properties at the interfaces and hence the surface area of the material is vital and discussed in the next section.

(c) BET Surface area of $CoMoO_4$

As the energy storage capability originating from the capacitive behaviour of the synthesised electrode depends on their specific area and pore volume, the pore structure and the presence of mesoporous were detected by N_2 adsorption–desorption.

Nitrogen adsorption-desorption isotherms and BJH pore size distribution (inset) for pure and modified $CoMoO_4$ samples are presented in Fig. 6. A typical N_2 adsorption-desorption graph for $CoMoO_4$ samples showing the rate of N_2 adsorption is higher with the increase in relative pressure. Both samples (Fig. 6a-b) show typical IV adsorption-desorption isotherm H_2 type hysteresis loops characteristics of mesoporous materials [28]. However, the area of the loop for the modified sample (Fig. 6b) is found to be quite higher than that for the pure $CoMoO_4$. This suggests the fact that the percentage of mesoporous particles is higher for the modified sample and as a result ion diffusion pathway is shorter for an intercalation reaction to occur reversibly. This favours the modified $CoMoO_4$ having enhanced pseudocapacitance for energy storage applications. As concluded in Table 1, the pure and modified $CoMoO_4$ has surface area of 11 and 20 $m^2\ g^{-1}$ respectively. The surface area of the pure sample was quite low without any hysteresis in the adsorption isotherm. A relatively high surface area obtained for the modified $CoMoO_4$ provides more faradaic active sites and facilitates the contact of the

active sites with the electrolyte. The modified sample possessing higher surface area compared to that of pure sample could be resulted from the fact that presence of polymeric surfactants during the synthesis controlled the particle size. Such unique nanostructure is highly desirable for faradaic and non-faradaic reactions occurring during charge-discharge processes for adsorption properties, fast ion diffusion and electron transportation [29]. The physico-chemical results strongly suggest the potential use of F127 added $CoMoO_4$ as a suitable cathode material for supercapacitor applications.

3.3. Electrochemical studies of $CoMoO_4$

(a) Cyclic Voltammetry studies

To evaluate the energy storage (capacitive) properties of the pure and modified $CoMoO_4$, potentiostatic cyclic voltammetry (CV), galvanostatic charge-discharge (CD), and electrochemical impedance spectroscopy (EIS) studies were carried out in aqueous 2 M NaOH electrolyte.

To acquire the redox peaks of pure and modified $CoMoO_4$ samples, cyclic voltammetric (CV) studies were initially carried out at scan rate of 1 mV s^{-1} and results are shown in Fig. 7A-B. As it is seen from Fig. 7A, oxidation (A1) and corresponding reduction peaks (C1 and C2) are quite weak and ill-defined indicating the pure cobalt molybdate material is less electrochemically active. However, for the modified sample (Fig. 7B), cyclic voltammogram shows a pair of strong redox peaks in each CV curves indicating a typical pseudocapacitive characteristic in nature that are mainly diffusion controlled, governed by faradic reactions. One well - defined oxidation (anodic) peak (A1 = 0.28 V) during the positive scan and while reversing the potential, in the negative scan, corresponding two reduction (cathodic) peaks (C1 = 0.11 and C2 = 0.53) are observed. A small shoulder (A2 = 0.45) is also seen during the oxidation reaction. The product formed during oxidation of the modified $CoMoO_4$ undergoes two separate reduction processes (C_1 and C_2) upon reversing

the potential. In the presence of F127 surfactant, the peak currents are prominent. Compared to pure sample the area under the peaks are much larger for the modified material, illustrating the material is electrochemically reversible and suitable for energy storage. The F127 non-ionic polymeric surfactant influences the electrolyte surface tension and improves the ionic transport that resulted in well-defined redox peaks and an additional shoulder A_2. The electrochemical performance indicates a better faradaic behaviour for the $CoMoO_4$ nanospheres within the voltage window of 0.6 V. A pair of redox peak (C_1 and A_1) seen in Fig. 7B is related to the formation of a different cobalt oxide indicating the pseudocapacitance behaviour is reversible for multiple cycles. The pseudocapacitance is correlated to the faradic process involving the ability of OH^- to be intercalated into the oxidised form of $CoMoO_4$ (Co_3O_4) for the improved charge storage. The electrochemical reactions of $CoMoO_4$ during oxidation (A1) and reduction (C1) could be summarised in equations 2-3 [8].

$$3[Co(OH)_3]^- \leftrightarrow Co_3O_4 + 4H_2O + OH + 2e^- \quad \text{Eq. (2)}$$

$$Co_3O_4 + H_2O + OH^- \leftrightarrow 3CoOOH + e^- \quad \text{Eq. (3)}$$

However, the peak C_2 raised from the adsorption of ions on the surface corresponding to the non-faradaic process is found to be quasi-reversible with a shoulder of A_2 during the subsequent oxidation process. The CV profile suggests that the addition of F127 onto $CoMoO_4$ leads to a change in surface functional groups having a carbon composites arise from the decomposition of polymeric surfactant at an elevated synthesis temperature of 300 °C. Figure 7C shows the cyclic voltammetric curves of the modified $CoMoO_4$ at different scan rates. At higher scan rates, the oxidation and reduction peaks are becoming more prominent suggesting fast kinetics and ease of ionic transport. The linear dependence of the current to the scan rates implies the capacitor is suitable for high power applications. The specific capacitance taken from the galvanostatic charge - discharge time within the voltage window

of 0.6 V was calculated for each scan rate and results are plotted in Fig. 7D and summarised in table 2. The inset in Fig. 7D showed the continuous charge discharge cycling between 0 and 0.6 V is reversible. The shape of the curves is a typical symmetrical shape without any distortion implying a capacitive behaviour with a 100% coulombic efficiency. The specific capacitance (SC) of the cobalt molybdate was calculated using the equation (4).

$$SC\ (F\cdot g^{-1}) = I\,\Delta t / m\,\Delta V \qquad \text{Eq. (4)}$$

Where *I (A)* is the applied current used for charge-discharge, Δt *(Sec)* is the time elapsed for the discharge cycle, *m (g)* is the mass of the active material and ΔV *(V)* is the voltage interval of the discharge.

From the three cell configuration, a specific capacitance of 170 F g^{-1} was observed for the modified $CoMoO_4$. However, the specific capacitance decreases as the current increases. This could be due to the faster sweep rate occurring on the surface rather in the bulk material at the higher discharge currents resulting in low transportation of ions.

(b) Charge – discharge studies of the hybrid capacitor (AC vs. $CoMoO_4$)

To further understand the capacitive behaviour of modified $CoMoO_4$ and to examine its suitability for energy storage device, a charge-discharge study was employed on the hybrid device. The term hybrid represents the combination of capacitive electrode (negative) and a faradaic electrode (positive), as shown in the schematic diagram Fig. 8A. Details on the electrochemical characteristics for the positive electrode ($CoMoO_4$) are shown in Fig. 7. The performance characteristics for the negative electrode, activated carbon (AC), have been shown in Fig. S3 (ESI§) and the results are in accordance with those reported in the literature [29]. Based on the three electrode configuration, the safe working voltage window for $CoMoO_4$ and AC electrodes are found to be 0.6 and 1.0 V, respectively. Hence, for the fabricated hybrid device (Fig. 8B), $CoMoO_4$ coupled with AC, the total cell working voltage should be 1.6 V. The energy density (E) was calculated using the equation (5).

$$E\ (Wh \cdot Kg^{-1}) = \text{Specific capacity}\ (mAh \cdot g^{-1}) \times \text{mid charge potential}\ (V) \quad \text{Eq. (5)}$$

Based on the initial results, galvanostatic studies of the device were performed only for modified $CoMoO_4$. Fig. 8B shows the charge-discharge characteristics of modified AC||$CoMoO_4$ at various current rates imposed on the device. The observed specific capacitance and energy densities at different currents for the device, AC||$CoMoO_4$, are tabulated in Table 3. The modified $CoMoO_4$ electrode delivers specific capacitance of 79, 76, 73 and 69 F g^{-1} at current of 0.1, 0.2, 0.5 and 1.0 A g^{-1}, respectively and maintains almost 90 % of its specific capacitance when the charge-discharge rate increases from 0.1 to 1.0 A.g^{-1}. The observed decrease in capacitance is linear with increasing current rate which is the typical behaviour of electrochemical capacitors. This capacity retention could be due to ion percolation (electrolyte penetration) on the large surface area of the mesoporous electrode and it is found to be versatile for multiple cycles.

Table 4 summarises the benchmark on the performance characteristics of the reported $CoMoO_4$ available and compared those results with our current work. The modified $CoMoO_4$ shows comparable electrochemical behaviour with those of the studies reported in Table 4. Moreover, the currently reported material is cost-effective and facile approach to that of microwave assisted synthesised samples and reduced graphite $CoMoO_4$ materials. This offers the modified $CoMoO_4$ presented in this study to be a possible candidate for future studies for next generation supercapacitors.

(c) Electrochemical Impedance Spectroscopy studies

Electrochemical impedance spectroscopy (EIS) was carried out in order to further ascertain the electrode/electrolyte interfacial resistance of the pure and modified $CoMoO_4$ electrodes. The Nyquist plots for pure and modified samples can be seen in Fig. 9A. At high frequency, the intercept of the semicircle with X axis represents the equivalent series resistance (ESR). ESR includes the ionic resistance of electrolyte, resistance of active material and resistance

between electrode and electrolyte. ESR value for modified electrode is almost 2 Ω cm^{-2} whereas the pure sample value is 29 Ω cm^{-2}. The lower value indicates faster charge-discharge ability of modified electrode than that of pure sample [16]. The diffusive resistance (Warburg impedance) of the modified electrode was lower than that of pure sample. The indicator is the straight line at the lower frequency region. The straight line at the low frequency region is due to diffusion of electrolyte ions. The closer is the line to 90^{o} (an indicator of an ideal supercapacitor) the better is the capacitance behaviour of the sample.

(d) Cycling stability of the hybrid capacitor ($CoMoO_4$ vs. AC)

To further examine the capacity retention of modified CoMoO4 vs. AC device, long term cycleability test over 2000 cycles was carried out and result is presented in Fig. 9B. A galvanostatic technique has been used to evaluate the cycling stability of the hybrid device. The modified $CoMoO_4$ material showed excellent cycling stability, after an initial decrease in capacitance, in the given potential window of 1.6 V while retaining almost 80% of its initial capacitance after 2000 cycles. The available discharge capacitance after 2000 cycles was about 60 F g^{-1}. The observed loss in capacitance is due to the reduced electron conductive carbon coating on the surface that increased ion diffusion resistance upon cycling. The continuous charge-discharge cycling curves for the first 100 cycles are shown in the inset, illustrating the shape of the curves have been retained and the electrochemical process involved both faradaic (electron transfer) and non-faradaic (adsorption) reactions. These results confirm the data obtained with BET measurements suggesting that the porous structure of the modified sample leads to reduce the mass transfer resistance and improves the penetration of the electrolyte and ion diffusion in the electrode material. Overall, the physico-chemical and electrochemical results suggests that the porous nature of the F127 added $CoMoO_4$ enhanced the performance through high ion diffusion and conductivity.

4. Conclusions

In summary, we have demonstrated the fabrication and performance of the polymeric surfactant added $CoMoO_4$ nanospheres. The F127 surfactant changes the rod-like structure of $CoMoO_4$ to nanospheres of 250 nm size. The surfactant–cobalt molybdate interaction favoured by the chosen concentration aids the growth of nanospheres with a carbon coating for good electronic conductivity. The mesoporous cobalt molybdate demonstrated a great pseudocapacitance and excellent cycling stability (almost 80% capacity retention over 2000 cycles) when utilised as electrode in a hybrid device *vs.* activated carbon electrode. The charge-discharge test revealed that surfactant assisted $CoMoO_4$ device had a specific capacitance of 79 F g^{-1} and energy density of 38 Wh Kg^{-1} at 1 mA current. The results confirm that unique morphology and mesoporous made the $CoMoO_4$ material suitable for next generation supercapacitors.

Acknowledgements

This research was funded from ARC's Discovery Projects funding scheme DP1092543.The views expressed herein are those of authors and are not necessarily those of the Australian Research Council. The authors would like to acknowledge Australian Synchrotron (P9499) for providing beam time to enable work on IR, Curtin University for SEM facilities and AINSE Research Grant (ALNGRA15051) to carry out the microscopy work at ANSTO.

References

1. L.Q. Mai, F. Yang, Y. L. Zhao, X. Xu, L. Xu and Y.Z. Luo, Hierarchical $MnMoO_4/CoMoO_4$ Hetrostructured Nanowires with Enhanced Supercapacitor Performance, Nature Commun. 2 (2011) 381-385.
2. M. C. Liu, L. B. Kong, X. J. Ma, C. Lu, X. M. Li, Y. C. Luo and L. Kang, Hydrothermal Process for the Fabrication of $CoMoO_4.0.9\ H_2O$ Nanorods with Excellent Electrochemical Behaviour, New J. Chem. 36 (2012) 1713-1716.

3. W. Chen, Z. Fan, L. Gu, X. Bao and C. Wang, Enhanced capacitance of manganese oxide via confinement inside carbon nanotubes, Chem. Commun. 46 (2010) 3905-3907.
4. J. Bae, M. K. Song, Y. J. Park, J. M. Kim, M. L. Liu and Z. L. Wang, Fibre Supercapacitors Made of Nanowire-Fibre Hybrid Structures for Wearable/Flexible Angew. Chem. Int. Ed. 50 (2011) 1683-1687.
5. P. Simon, Y. Gogotsi, Materials for electrochemical capacitors, Nat. Mater. 7 (2009) 845 - 854.
6. M. Mandal, D. Ghosh, S. Giri, I. Shakir, and C. K. Das, Polyaniline-Wrapped 1D $CoMoO_4$. 0.75 H_2O Nanorods as Electrode Material for Supercapacitor Energy Storage Applications, RSC Adv. 4 (2014) 30832-30839.
7. L. Hou, H. Hua, S. Liu, G. Pang, and C. Yuan, Surfactant-Assisted Hydrothermal Synthesis of Ultrafine $CoMoO_4$.0.9 H_2O Nanorods Towards High-Performance Supercapacitors, New. J. Chem. 39 (2015) 5507-6177.
8. R. Ramkumar, M. Minakshi, Fabrication of ultrathin $CoMoO_4$ nanosheets modified with chitosan and their improved performance in energy storage device, Dalton Trans. 44 (2015) 6158-6168.
9. J. Candler, T. Elmore, B. K. Gupta, L. Dong, S. Palchoudhury and R. K. Gupta, New Insight into High-Temperature Driven Morphology Reliant $CoMoO_4$ Flexible Supercapacitors, New. J. Chem. 39 (2015) 6108-6116.
10. J. Zheng, P. J. Cygan and T. R. Jow, Hydrous ruthenium oxide as an electrode material for electrochemical capacitors, J. Electrochem. Soc. 142 (1995) 2699-2703.
11. H. Wang, L. Zhang, X. Tan, C. M. B. Holt, B. Zahiri, B. C. Olsen and D. Mitlin, Supercapacitive Properties of Hydrothermally Synthesised Co_3O_4 Nanostructures, J. Phys. Chem. C 115 (2011) 17599-17605.
12. G. Han, Y. Liu, L. Zhang, E. Kan, S. Zhang, J. Tang and W. Tang, MnO_2 Nanorods Intercalating Graphene Oxide/Polyaniline Ternary Composites for Robust High-Performance Supercapacitors, Sci. Rep. 4 (2014) 4824-4830.
13. M. Minakshi, P. Singh, D. Appadoo and D. E. Martin, Synthesis and characterization of olivine $LiNiPO_4$ for aqueous rechargeable battery, Electrochim. Acta 56 (2011) 4356-4360.
14. M. Minakshi, P. Singh, N. Sharma, M. Blackford and M. Ionescu, Lithium extraction−insertion from/into $LiCoPO_4$ in aqueous batteries, Ind. Eng. Chem. Res. 50 (2011) 1899-1905.

15. M. Minakshi, A. Pandey, M. Blackford and M. Ionescu, Effect of TiS_2 additive on $LiMnPO_4$ cathode in aqueous solutions, Energy & Fuels 24 (2010) 6193-6197.
16. Z. Xu, Z. Li, X. Tan, C. M. B. Holt, L. Zhang, B. Sh. Amirkhiz and D. Mitlin, Supercapacitive carbon nanotube-cobalt molybdate nanocomposites prepared via solvent-free microwave synthesis, RSC Adv. 2 (2012) 2753-2755.
17. X. Xu, J. Shen, N. Li and M. Ye, Microwave-assisted synthesis of graphene/$CoMoO_4$ nanocomposites with enhanced supercapacitor performance, Journal of Alloys and Compd. 616 (2014) 58-65.
18. S. Baskar, D. Meyrick, K. S. Ramakrishnan and M. Minakshi, Facile and large scale combustion synthesis of a-$CoMoO_4$: mimics the redox behaviour of a battery in aqueous hybrid device, Chem. Eng. J. 253 (2014) 502-507.
19. Y. Ding, C. F. Xia, H. Zhou, L. Wang and X. l. Hu, Influence of sintering temperature on the structural and morphological performance of $CoMoO_4$, Russian J. Inorg. Chem. 57 (2012) 569-573.
20. B. Das, M. V. Reddy, S. Tripathy and B. V. R. Chowdari, A disc-like Mo-metal cluster compound, $Co_2Mo_3O_8$, as a high capacity anode for lithium ion batteries, RSC Adv. 4 (2014) 33883-33889.
21. D. Guo, H. Zhang, X. Yu, M. Zhang, P. Zhang, Q. Li, T. Wang, Facile synthesis and excellent electrochemical properties of $CoMoO_4$ nanoplate arrays as supercapacitors, J. Mater. Chem. A 1 (2013) 7274-7254.
22. Z. Zhang, Y. Liu, Z. Huang, L. Ren, X. Qi, X. Wei and J. Zhong, Facile hydrothermal synthesis of $NiMoO_4$@$CoMoO_4$ hierarchical nanospheres for supercapacitor applications, Phys. Chem. Chem. Phys. 17 (2015) 20795-20804.
23. R. Zhang and P. Somasundaran, Advances in adsorption of surfactants and their mixtures at solid/solution interfaces, Adv. Colloid Interface Sci. 123- 126 (2006) 213 – 229.
24. R. L. Frost, J. Cejka and M. J. Dickfos, Raman and infrared spectroscopic study of the molybdate uranyl mineral calcurmolite, J. Raman Spectroscopy 39 (2008) 779 – 785.
25. Y. Wan and D. Zhao, On the Controllable Soft-Templating Approach to Mesoporous Silicates, Chem. Rev. 107 (2007) 2821 – 2860.
26. T. Sen, G. J. T. Tiddy, J. L. Casci and M. W. Anderson, Synthesis and characterization of hierarchically ordered porous silica materials, Chem. Mater. 16 (2004) 2044 – 2054.

27. R. Wang, X. Yan, J. Lang, Z. Zheng, and P. Zhang, J. Mater. A hybrid supercapacitor based on flower like Co $(OH)_2$ and urchin like electrode materials, Chem. A. 2 (2014) 12724-12732.
28. M. Q. Yu, L. X. Jiang and H. G. Yang, Ultrathin nanosheets constructed $CoMoO_4$ porous flowers with high activity for electrocatalytic oxygen evolution, Chem. Commun. 51 (2015) 14361-14364.
29. M. Minakshi, D. Meyrick, D. Appadoo, Maricite $(NaMn_{1/3}Ni_{1/3}Co_{1/3}PO_4)$/activated carbon: Hybrid capacitor, Energy Fuels 27 (2013) 3516-3522.
30. B. Senthilkumar, K. V. Sankar, R. Kalai Sevlan, D. Meyrick and M. Minakshi, Nano a-$NiMnO_4$ as a new electrode for electrochemical supercapacitors, RSC Adv. 3 (2013) 352-357.
31. G. K. Veerasubramani, K. Krishnamoorthy, S. Radhakrishnan, N. Kim and S. J. Kim, Synthesis, characterization, and electrochemical properties of $CoMoO_4$ nanostructures, Int. J. Hydrogen Energy 39 (2014) 5186-5193.

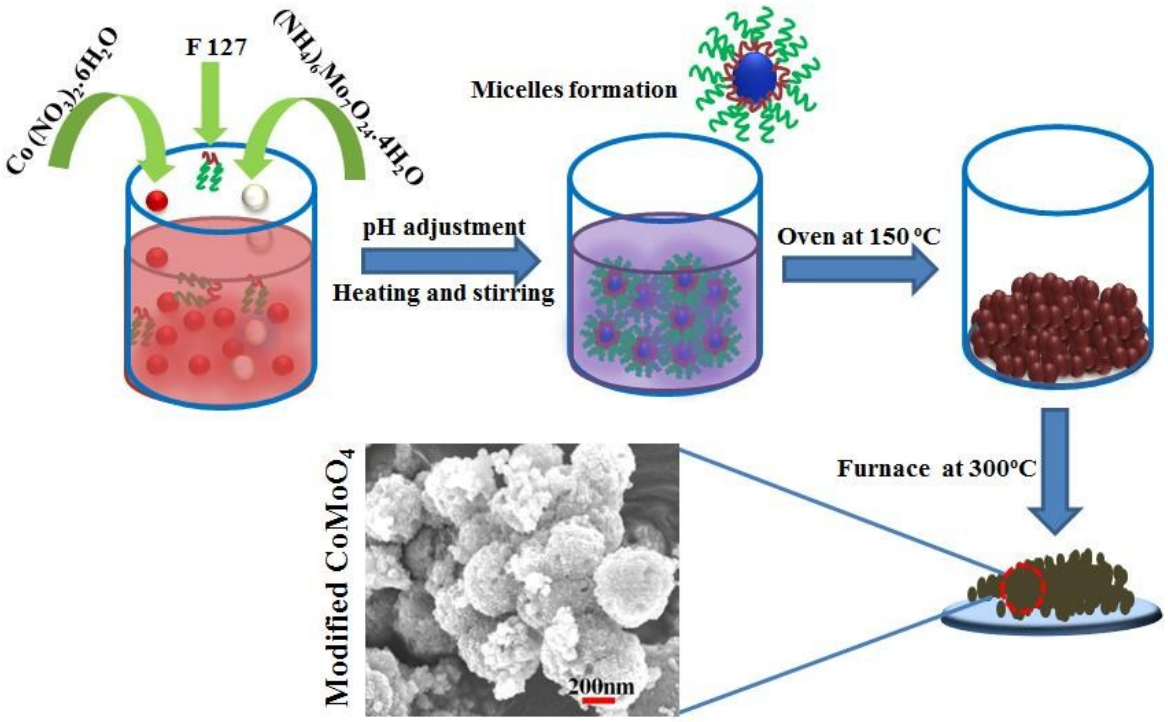

Figure 1 Schematic representation of the synthesis of $CoMoO_4$ sample.

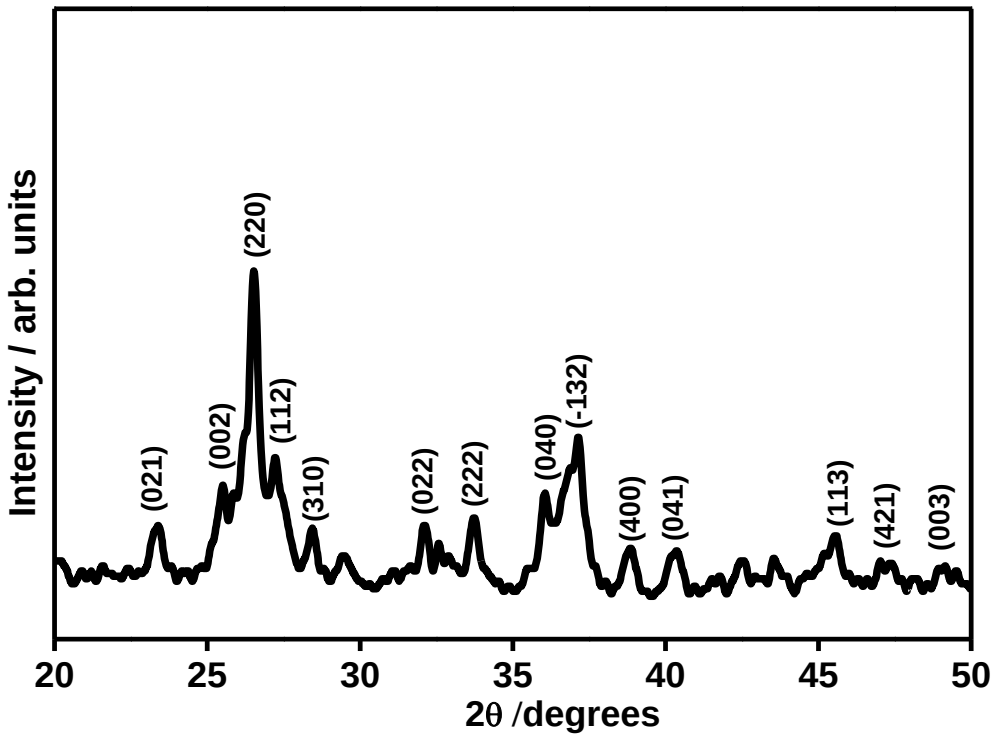

Figure 2 X-ray diffraction (XRD) pattern of the modified $CoMoO_4$ sample.

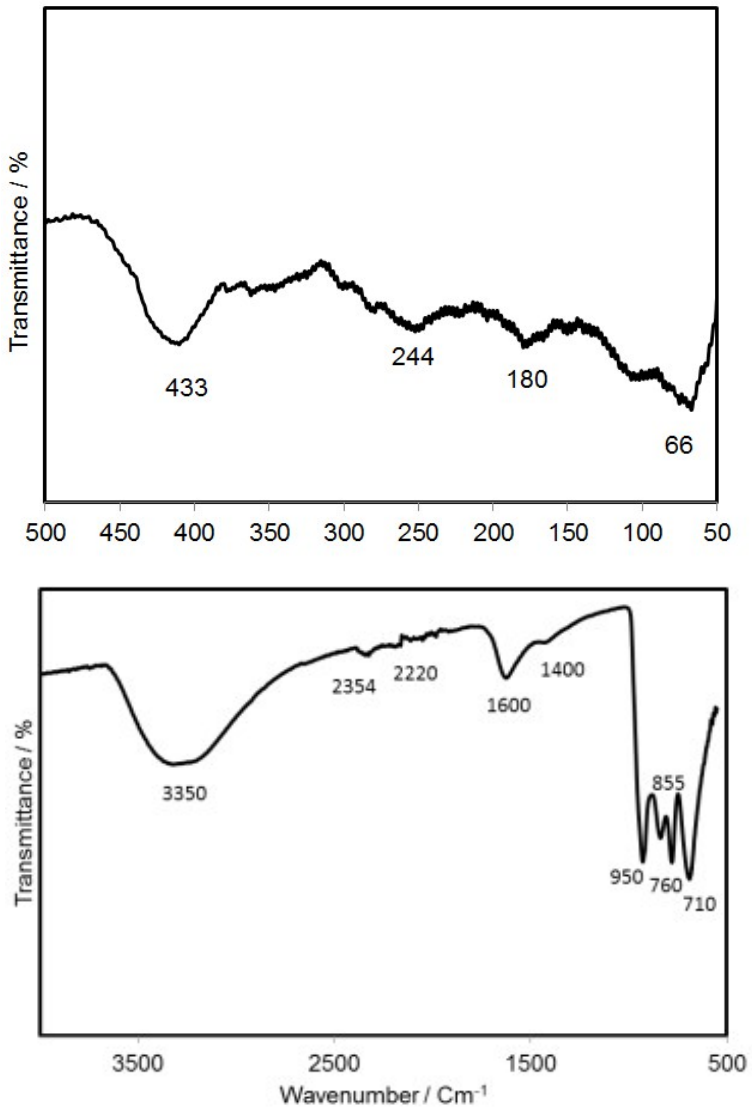

Figure 3 The far (A) and mid (B) infrared transmittance spectra (IR) of the modified $CoMoO_4$ material using synchrotron source.

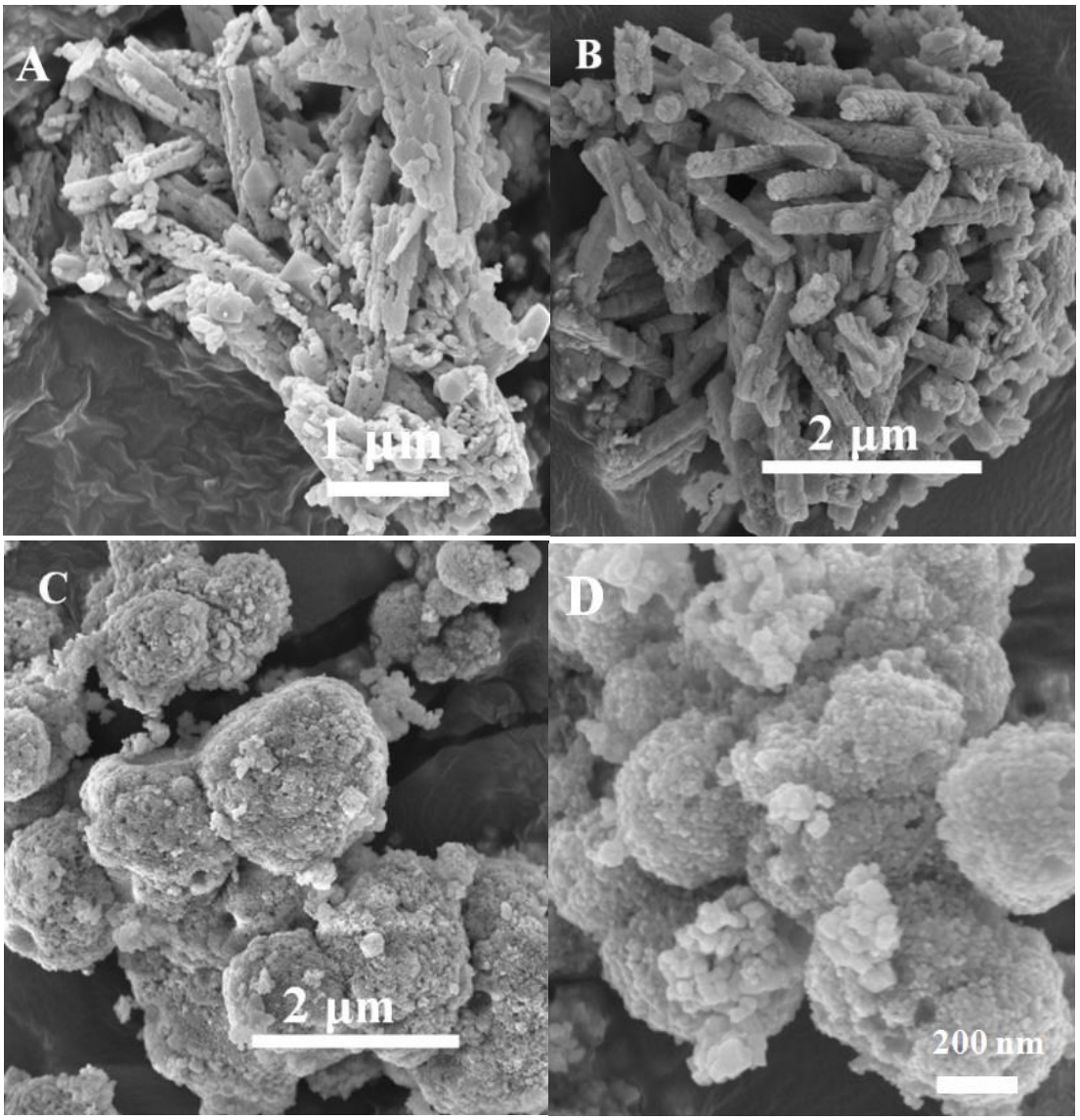

Figure 4 Field emission SEM micrographs of (A-B) pure and (C-D) modified (F127 added) $CoMoO_4$ at a lower and higher magnifications.

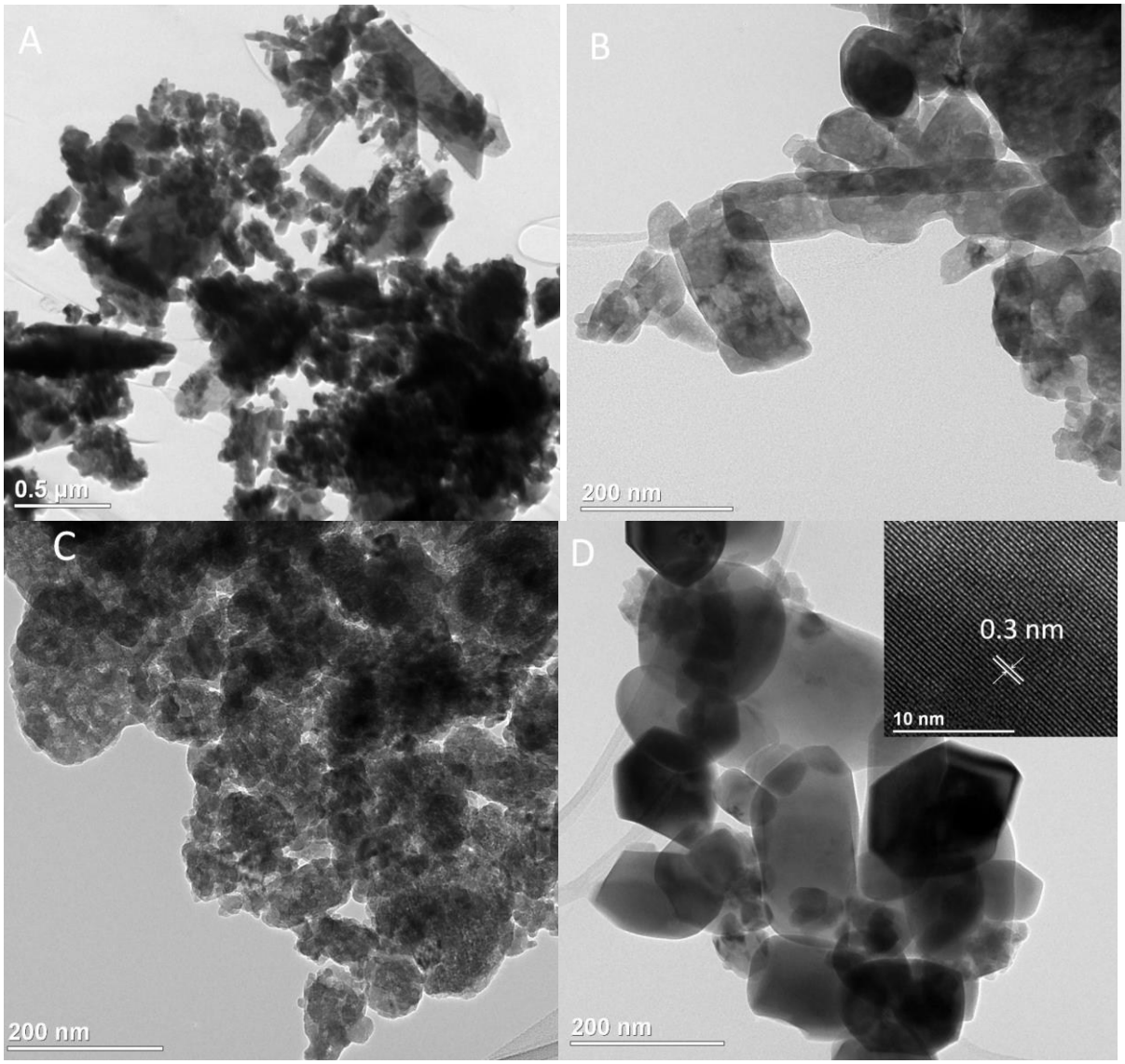

Figure 5 TEM imaging of (A-B) pure and (C-D) modified (F127 added) $CoMoO_4$ at a lower and higher magnifications. (d) represents a hexagonal shaped particle. An inset has been shown in Fig. 5d indicating fringes like pattern relating $CoMoO_4$ particles.

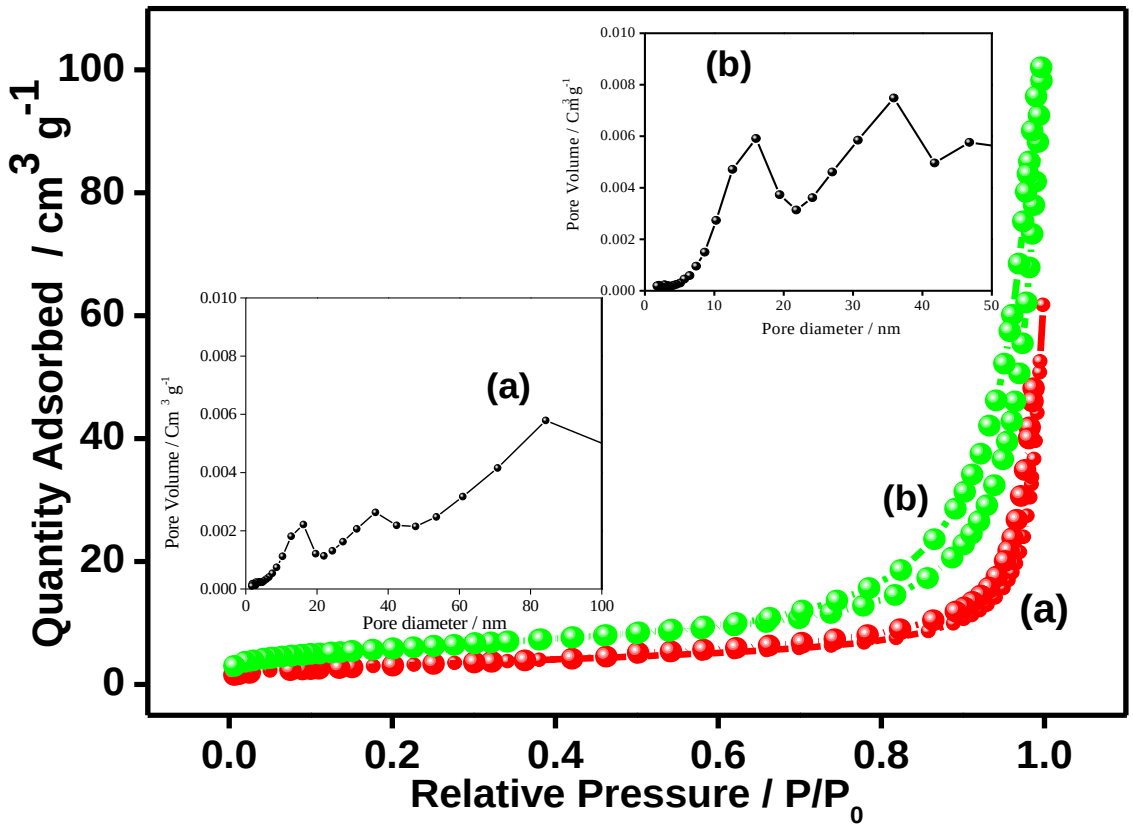

Figure 6 Nitrogen adsorption-desorption isotherms of (a) pure and (b) modified $CoMoO_4$ samples. Insets are pore-size distribution curves.

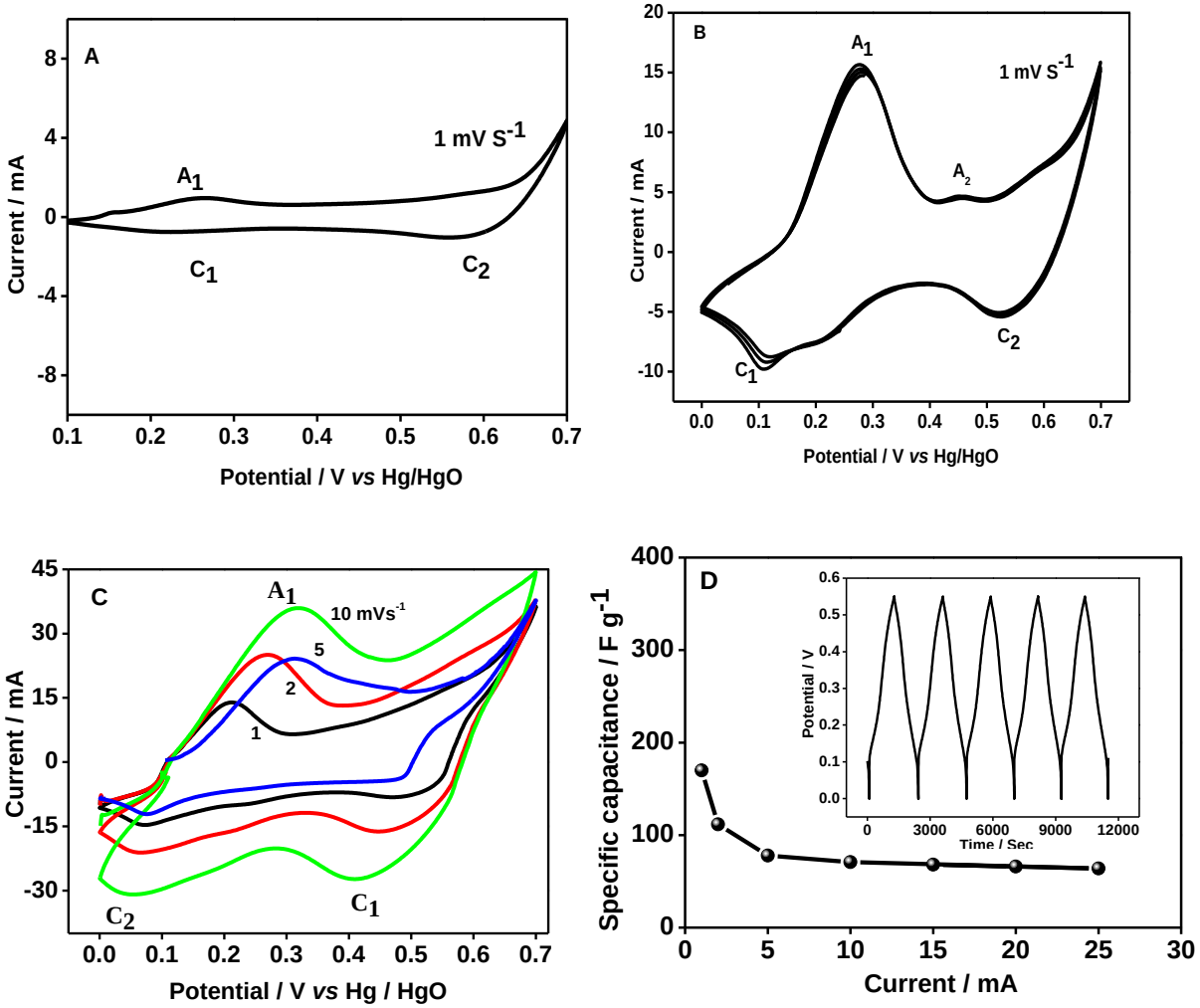

Figure 7 Cyclic voltammetric curves of (A) pure and (B) modified $CoMoO_4$. (C) CV curves of modified $CoMoO_4$ at variable sweep rates (indicated in the figure). (D) variation of specific capacitance with current for modified $CoMoO_4$, Inset in (d) shows the charge-discharge cycles (for 20, 40, 60, 80 and 100 cycles) illustrating the reversibility of the cell tested in three-cell configuration.

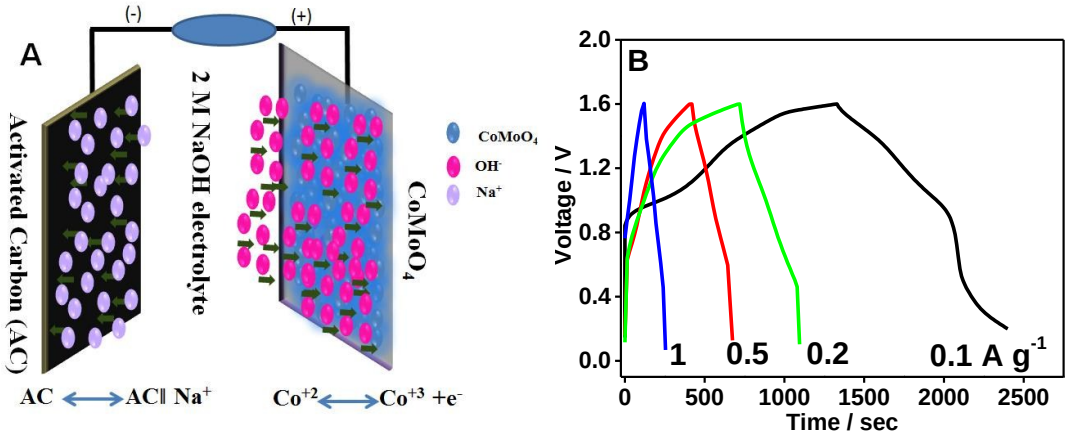

Figure 8 (A) schematic representation of hybrid device fabricated in this study and (b) galvanostatic charge-discharge profiles of modified $CoMoO_4$ tested at different currents.

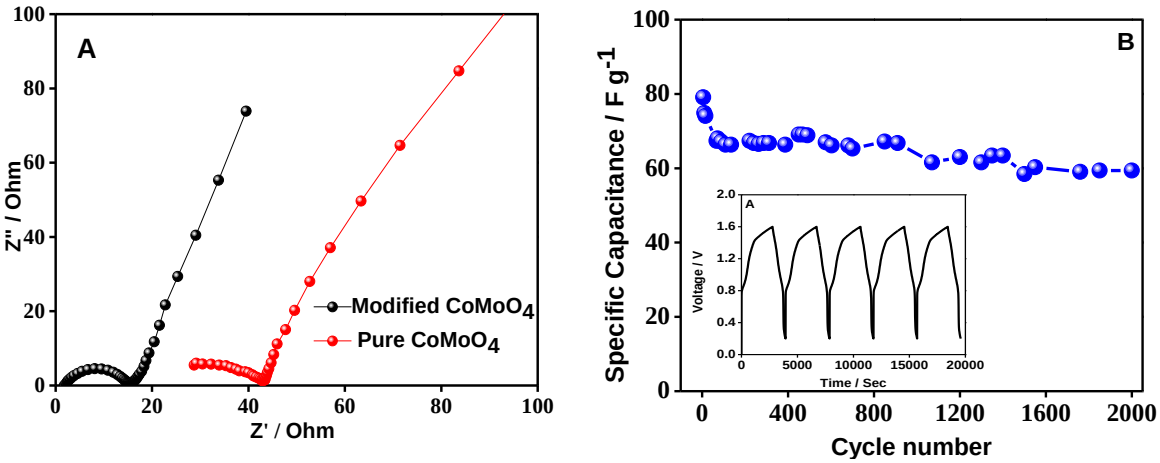

Figure 9 (A) Electrochemical Impedance Spectra (EIS) of pure and modified $CoMoO_4$ materials. (B) variation of specific capacitance *vs.* cycle number for modified $CoMoO_4$ material. Inset shows the charge-discharge cycles (for 20, 40, 60, 80 and 100 cycles) illustrating the reversibility of the device tested in two-cell configuration.

Table 1 Physical property of pure and modified $CoMoO_4$ samples

Sample	BET surface area, $m^2\ g^{-1}$	Average particle size, nm	Average pore diameter, nm
pure	11.4	525.5	29.2
modified	20.8	288	30.6

Table 2 Calculated specific capacitance for modified $CoMoO_4$ obtained through the potentiodynamic method at different sweep rates

Scan rate /mV S^{-1}	**1**	**2**	**5**	**10**	**25**
Specific capacitance/ F g^{-1}	170	111	78	71	64

Table 3 Calculated specific capacitance and energy densities for modified AC||$CoMoO_4$

Specific current / A ·g^{-1}	Specific capacitance / F g^{-1}	Energy density / W h Kg^{-1}
0.1	79	38
0.2	76	33
0.5	73	31
1.0	69	29

Table 4 Comparison of the electrochemical performance of $CoMoO_4$ material

Electrode material	Specific capacitance/ F g^{-1}	Electrolyte	Configuration (two/three electrode)	Reference
$MnMoO_4/CoMoO_4$	187.1	2M NaOH	3	[1]
$CoMoO_4.0.75\ H_2O$	380	1 M Na_2SO_4	3	[5]
$CoMoO_4$.Chitosan	135	2 M NaOH	2	[8]
$CoMoO_4$	169	3 M KOH	3	[9]
$CoMoO_4$/MWCNTs	170	2 M NaOH	3	[16]
RGO/$CoMoO_4$	322.5	6 M NaOH	3	[17]
$CoMoO_4$	105	2 M Li(OH)	2	[18]
$NiMoO_4$-$CoMoO_4.X\ H_2O$	80	2 M NaOH	2	[30]
$CoMoO_4$	133	2 M KOH	3	[31]
$CoMoO_4$	170	2 M NaOH	3	This study
$CoMoO_4$	79	2 M NaOH	2	This study

Table of Content

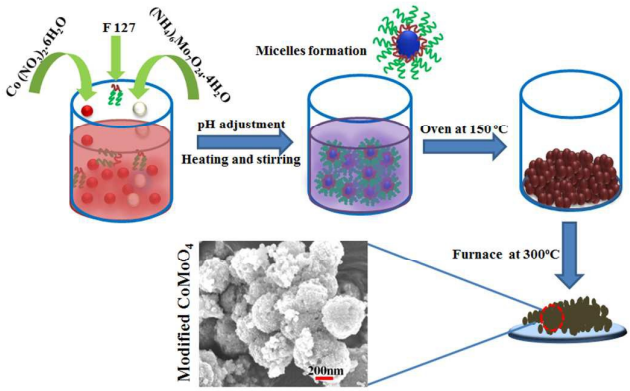

The role of Pluronic F127 onto $CoMoO_4$ and its influence on the electrochemical energy storage have been reported.